Appl. Phys. B 84, 97–101 (2006)
DOI: 10.1007/s00340-006-2211-4

Applied Physics B
Lasers and Optics

M. REICHELT[1,✉]
S.W. KOCH[2]
A.V. KRASAVIN[3]
J.V. MOLONEY[1]
A.S. SCHWANECKE[3]
T. STROUCKEN[2]
E.M. WRIGHT[4]
N.I. ZHELUDEV[3]

Broken enantiomeric symmetry for electromagnetic waves interacting with planar chiral nanostructures

[1] Arizona Center for Mathematical Sciences, University of Arizona, Tucson, AZ 85721, USA
[2] Department of Physics and Material Sciences Center, Philipps-University, Renthof 5, 35032 Marburg, Germany
[3] EPSRC NanoPhotonics Portfolio Centre, School of Physics and Astronomy, University of Southampton, SO17 1BJ, UK
[4] College of Optical Sciences, University of Arizona, Tucson, AZ 85721, USA

Received: 8 December 2005
Published online: 19 April 2006 •

ABSTRACT Simulations of Maxwell's equations for electromagnetic waves interacting with planar chiral structures are shown to depend on the polarization state of the exciting light field. These results illustrate generic features of light interaction with planar chiral structures and imply broken enantiomeric symmetry for excitation with circularly polarized light.

PACS 78.67.-n; 11.30.-j

1 Introduction

A chiral object exhibits a left–right asymmetry, such that the object cannot be brought into congruence with its mirror image. Chiral objects can exist in two forms that are otherwise identical left and right mirror images known as enantiomeric forms. An optical manifestation of chirality is the ability to rotate the polarization state of light in a fashion sensitive to the handedness of the object, which is known as optical activity. Although conventionally chirality is considered in three dimensions, a planar structure is said to be chiral if it cannot be brought into congruence with its mirror image unless it is lifted from the plane. Regular planar chiral structures (PCS) are rare in nature and only recently have become the subject of experimental investigations [1–3]. In particular, recent microscope observations of metallic PCSs composed of fourfold gammadion structures[1] revealed unusual anti-symmetries of the polarized images [2] in reflection. Furthermore, several experiments have reported polarization rotation of light diffracted from [1] and transmitted through [3] planar chiral nanostructures, showing that the chiral properties of the gammadions comprising the PCSs can affect the polarization state of light scattered from them in a fashion sensitive to the direction of twist. Recent theoretical studies examined boundary conditions at chiral interfaces [4] and polarization eigenstates in far-field diffraction from PCSs [5].

✉ Fax: +1-520-621-1510, E-mail: reichelt@acms.arizona.edu

[1] A gammadion is a star-like structure consisting of several rays or arms resembling the Greek capital letter gamma Γ. It possesses a center of rotation. Here and below we investigate gammadions with fourfold rotational symmetry.

In this article we investigate to which extent the symmetry of the light–matter interaction can result from the planar chiral patterning of the structure alone, i.e., without reference to the specific properties of the material itself. We demonstrate using Maxwell's equations that broken enantiomeric symmetry and sensitivity to the light polarization state are directly related to each other and are generic properties of electromagnetic wave interactions with PCSs. In Sect. 2, we investigate structures of fourfold gammadions by numerically solving Maxwell's equations for various excitation conditions. The structures considered are assumed to be either purely dielectric or metallic, i.e., containing loss mechanisms. In both cases we observe broken enantiomeric symmetry if the gammadions are illuminated with circularly polarized light, and this challenges the conventional wisdom that electromagnetic wave interactions with nonmagnetic and locally isotropic media are independent of the polarization state of the exciting light field. In Sect. 3, we elucidate our numerical calculations using formal solution of Maxwell's equations, and it is shown that, within the paraxial approximation, the flow maps exhibit the same symmetry properties as the PCS, independent of the polarization state of the exciting light field, whereas beyond the paraxial approximation the flow maps reflect the combined symmetries of the PCS and the exciting light field. Section 4 gives an alternative view of the polarization coupling that appears beyond the paraxial approximation, and finally Sect. 5 summarizes our conclusions.

2 Numerical simulations

Our numerical simulations are based on the three-dimensional macroscopic Maxwell's equations for the electric field $\boldsymbol{E}$ and the magnetic induction $\boldsymbol{B}$

$$\nabla \times \boldsymbol{E} = -\dot{\boldsymbol{B}}, \quad \nabla \times \boldsymbol{H} = \dot{\boldsymbol{D}}\,,$$
$$\nabla \cdot \boldsymbol{D} = 0, \quad \nabla \cdot \boldsymbol{B} = 0\,, \tag{1}$$

along with the constitutive relations $\boldsymbol{B} = \mu_0 \boldsymbol{H}$ for a nonmagnetic medium, and the electric displacement

$$\boldsymbol{D}(\boldsymbol{r}, t) = \varepsilon_0 \left(\boldsymbol{E}(\boldsymbol{r}, t) + \int \mathrm{d}t'\, f(\boldsymbol{r}) \chi^R(t - t') \boldsymbol{E}(\boldsymbol{r}, t') \right). \tag{2}$$

Here $\chi^R(t)$ is the retarded linear susceptibility for the structure and $f(\boldsymbol{r})$ reflects the patterning of the PCS. We assume that

the medium is everywhere locally isotropic so that the susceptibility is a scalar function. For the case considered here of a fourfold planar gammadion, we have the symmetry properties $f(\boldsymbol{r}) = f(\mathcal{D}_{n\pi/2}\boldsymbol{r})$ and $f(\mathcal{M}\boldsymbol{r}) = f_{\mathcal{R}}(\boldsymbol{r})$ where $\mathcal{D}_{\varphi}$ denotes a rotation in the plane of the PCS, $\mathcal{M}$ refers to a reflection at a line in the plane and $f_{\mathcal{R}}$ to the patterning of the enantiomeric structure.

Figure 1 shows an array of fourfold gammadions with its left-hand (**L**) and right-hand (**R**) form, respectively, i.e., **L** is the enantiomer of **R** and vice versa. Here, we modeled the structures assuming an instantaneous, piecewise constant dielectric function. In the dark areas, $\chi(t) = 0$, corresponding to vacuum, and $\chi(t) = 12\delta(t)$ in the slab area. The simulations were performed using the standard finite-difference time-domain (FDTD) method [6] to solve Maxwell's equations, (1), with periodic boundary conditions, i.e., we consider an infinite two-dimensional array of gammadions. In the present case the film thickness is 175 nm, the groove width 450 nm, and the unit-cell length is 2500 nm. This model with an instantaneous response corresponds to a lossless medium.

Alongside each structure in Fig. 1 we have placed the flow maps (FM) of the reflected light obtained as the normal projection of the total Poynting vector $\boldsymbol{S} = \boldsymbol{E} \times \boldsymbol{H}$ onto the incident light propagation direction. The PCS is excited with a linearly polarized ultra-short pulse having a temporal width of about 10 fs and the reflection is recorded in the near field approximately 0.6λ ($\lambda \approx 800$ nm) above the surface. For all figures the dark background of the FMs refers to low intensity while brighter areas generally stand for higher intensities. More accurate perception can be achieved in the online color coded version where increasing intensity is represented as color change from blue over yellow to red. Examination of the FMs in Fig. 1 for linearly polarized excitation clearly shows that the FM of the enantiomer is the mirror image of the FM of the original structure, but loses its fourfold rotation symmetry. The latter has also been observed experimentally in [2].

In contrast, the FMs lose their mirror symmetry but retain their fourfold rotation symmetry if the structures are excited with circularly polarized light, as can be seen in Fig. 2. The upper part of Fig. 2 shows the FMs of the left hand gammadion as shown in Fig. 1 excited with left circularly polarized light (upper left), and right circularly polarized light (upper right), respectively. The lower part of Fig. 2 shows the corresponding FMs of the right hand gammadion for identical excitation conditions. It is clearly observable that the FMs of the enantiomers excited with circularly polarized light of the same handedness are no longer mirror images of each other. Instead, the mirror symmetry is conserved when comparing the PCS with opposite chirality and opposite light polarization, i.e., the FMs top left and down right as well as top right and down left are mirror images.

To generalize beyond our model of purely dielectric material, we have also performed numerical simulations using the finite element frequency-domain (FEM) method to solve for the electromagnetic fields associated with an individual fourfold chiral gammadion opening in a metallic film analogous to those employed in the experiment of [2]. In this approach Maxwell's equations are solved in the frequency domain along with the constitutive relation $\boldsymbol{D}(\boldsymbol{r}, \omega) = \varepsilon(\boldsymbol{r}, \omega) \cdot \boldsymbol{E}(\boldsymbol{r}, \omega)$, where at frequency ω_0 the space and frequency-dependent dielectric constant $\varepsilon(\boldsymbol{r}, \omega)$ is obtained via the Fourier transform of $\varepsilon(\boldsymbol{r}, t)$. The shape of the gammadion is shown as the dashed-line in Fig. 3a, which we take as our reference scenario. In each of the scenarios plotted in Fig. 3 a cir-

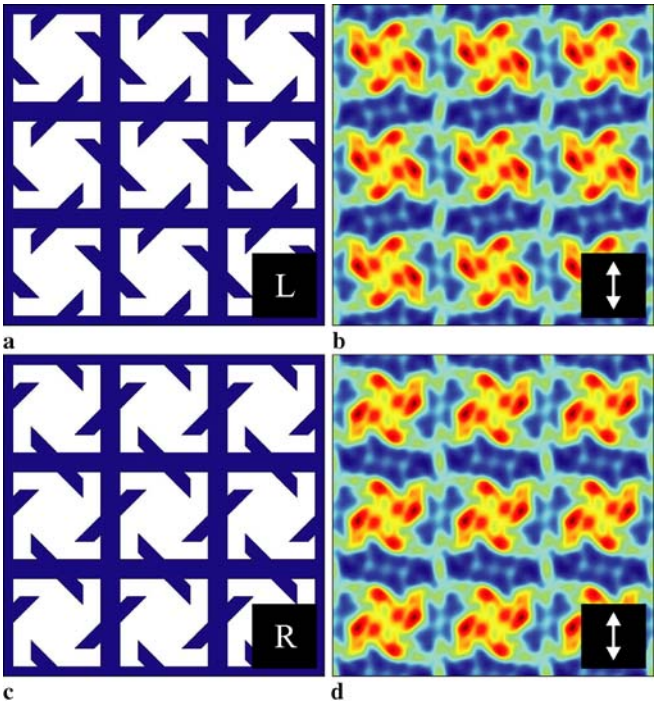

FIGURE 1 (color online) *Left-hand side*: Top view of two PCSs where **L** is the enantiomer of **R**. *Right-hand side*: Corresponding FMs when exciting the structures with linearly polarized light as indicated by the *arrows*

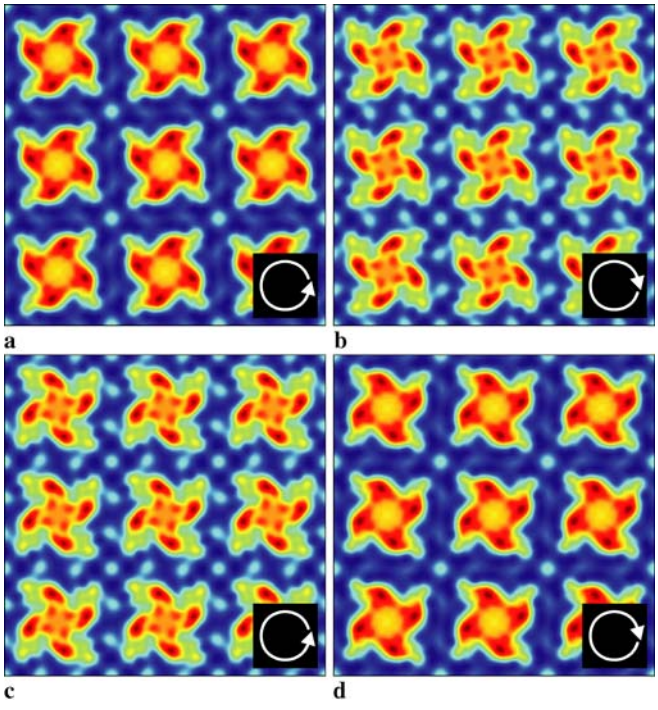

FIGURE 2 (color online) FMs of the reflected light by the PCSs **L** and **R**, see Fig. 1, when illuminating the structures with circularly polarized light as as indicated by the *arrows*

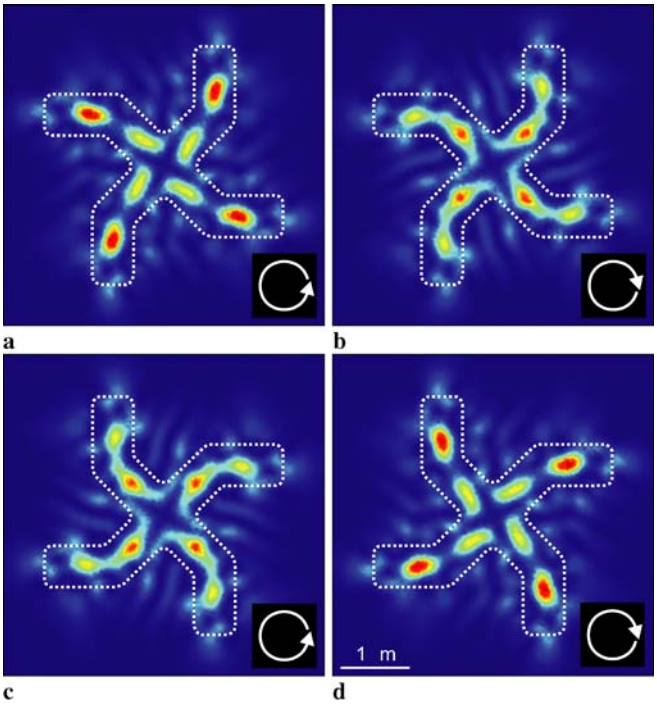

FIGURE 3 (color online) Taking example (**a**) as our reference scenario, where a clockwise polarized field is incident on a anti-clockwise PCS, we illustrate the actions of (**b**) reversing the incident polarization, (**c**) reversing the PCS handedness, and (**d**) reversing both the incident polarization and the handedness of the PCS. The *dashed line* indicates the shape of the gammadion

cularly polarized field of the indicated handedness is incident onto the gammadion traveling into the page, and for variety we here plot the electric field intensity after the generated EM fields have passed through a cross-circularly polarized filter of opposite handedness. The gammadion is a 140 nm thick gold film, with dielectric constant $\varepsilon(\boldsymbol{r}, \omega = \omega_0) = -8.68 - 1.2\mathrm{i}$ for an incident frequency $\omega_0 = 3 \times 10^{15}\mathrm{rad\,s^{-1}}$, with the gold removed from the region inside the dashed line in Fig. 3a, all non-gold regions being treated as vacuum $\varepsilon(\boldsymbol{r}, \omega_0) = 1$. The complex, frequency dependent dielectric constant for gold indicates that its linear response is lossy and no longer instantaneous. Figure 3b and c show the effects of reversing the handedness of the incident field and the PCS chirality, respectively, with respect to the reference scenario, and clearly the electric field intensity is different. In contrast, if we reverse both the handedness of the incident field and the twist of the medium as shown in Fig. 3d, then the electric field intensity is indistinguishable to the mirror image of the reference scenario. Thus, the conclusion drawn for the example of the dielectric PCS that the interaction between the PCS and light is sensitive to the polarization state of the incident light is seen also to apply to the lossy metallic PCS. From these examples we see that broken enantiomeric symmetry is a generic property of planar chiral structures.

3 Analytical considerations

To substantiate our numerical findings we analyze analytically the general symmetry properties of the FMs as obtained from Maxwell's equations. For this purpose, we start from the wave equation for the electric field in frequency space

$$\nabla \times \nabla \times \boldsymbol{E} - \frac{\omega^2}{c^2}\boldsymbol{E} = \frac{\omega^2}{c^2} f(\boldsymbol{r})\chi(\omega)\boldsymbol{E}(\boldsymbol{r}, \omega)\,, \tag{3}$$

and determine the magnetic field from Faraday's law

$$\boldsymbol{H}(\boldsymbol{r}, \omega) = -\frac{\mathrm{i}}{\mu_0 \omega}\nabla \times \boldsymbol{E}(\boldsymbol{r}, \omega)\,. \tag{4}$$

The FM is obtained as the normal projection of the Poynting vector, which is given in frequency space by

$$\begin{aligned}\boldsymbol{n} \cdot \boldsymbol{S}(\boldsymbol{r}, \omega) &= \frac{1}{2}\boldsymbol{n} \cdot (\boldsymbol{E}^*(\boldsymbol{r}, \omega) \times \boldsymbol{H}(\boldsymbol{r}, \omega)) + c.c. \\ &= \Im \frac{1}{\mu_0 \omega}\boldsymbol{n} \cdot \left(\sum_i E_i^* \nabla E_i - (\boldsymbol{E}^* \cdot \nabla)\boldsymbol{E}\right)\end{aligned} \tag{5}$$

In the following, we shall view the right-hand side of (3) as a source term. A formal solution of (3) including the proper initial/boundary conditions is then obtained with the aid of the Green tensor corresponding to the homogeneous wave equation [7] on the left-hand-side of (3):

$$\begin{aligned}\boldsymbol{E}(\boldsymbol{r}, \omega) &= \boldsymbol{E}_0(\boldsymbol{r}, \omega) \\ &\quad + \frac{\omega^2}{c^2}\int \mathrm{d}^3 r' \underline{\underline{G}}(\boldsymbol{r} - \boldsymbol{r}', \omega) f(\boldsymbol{r}')\chi(\omega)\boldsymbol{E}(\boldsymbol{r}', \omega) \\ &= \boldsymbol{E}\left[\boldsymbol{E}_0(\boldsymbol{r}, \omega),\ f(\boldsymbol{r})\right].\end{aligned} \tag{6}$$

Thus, the total field of the interacting system can be seen as a functional of the incident field $\boldsymbol{E}_0(\boldsymbol{r}, \omega)$ and the patterning of the chiral structure as reflected in the scalar function $f(\boldsymbol{r})$. The integral signifies non-local relations between the field interacting with the structure and is taken over the full domain of the associated integration variable.

In frequency space the Green tensor can be expressed as

$$\underline{\underline{G}}(\boldsymbol{r}, \omega) = \left(\underline{\underline{I}} + \frac{c^2}{\omega^2}\nabla \otimes \nabla\right)\mathcal{G}(\boldsymbol{r}, \omega)\,, \tag{7}$$

$$\mathcal{G}(\boldsymbol{r}, \omega) = \frac{1}{4\pi r}\mathrm{e}^{\mathrm{i}\omega r/c}, \tag{8}$$

where $\mathcal{G}$ is the Green function of the scalar wave equation and $\underline{\underline{I}}$ the unit tensor. The first term on the RHS of (7) corresponds to the solution of the scalar wave equation, whereas the second term accounts for non-paraxial contributions proportional to $\nabla(\nabla \cdot \boldsymbol{E})$, which can be seen by partially integrating the RHS of (6) and using $\nabla \cdot \boldsymbol{D} = \varepsilon_0(\nabla \cdot \boldsymbol{E} + \chi \nabla \cdot f(\boldsymbol{r})\boldsymbol{E}) = 0$. We refer to such terms as non-paraxial since they only contribute significantly if the patterning of the PCS varies on the scale of the optical wavelength, otherwise one may approximate $\nabla \cdot \boldsymbol{E} = 0$ as in the usual paraxial approximation where the electric field is treated as strictly transverse [8]. (Another view of the non-paraxial terms will be given in the next section).

Next we turn to the symmetry properties of the electric and magnetic fields under in-plane rotations and mirror inversion at a line in the plane of the PCS. To set the stage for studying the symmetries we first investigate the symmetry properties within the paraxial approximation. First we notice

that due to the diagonal character of the Green tensor in the paraxial approximation, the polarization state of the initial field is conserved so that there is no polarization conversion and the paraxial approximation predicts a dark FM in cross-polarization. Furthermore, for normal incident light, we have $\boldsymbol{n}\cdot\boldsymbol{E}=\boldsymbol{n}\cdot\boldsymbol{E_0}=0$, so only the first term on the RHS of (5) contributes to the FM. Since the scalar Green function is obviously invariant both under rotations and mirror inversion, i.e., $\mathcal{G}(\mathcal{D}_\varphi\boldsymbol{r},\omega)=\mathcal{G}(\mathcal{M}\boldsymbol{r},\omega)=\mathcal{G}(\boldsymbol{r},\omega)$, we obtain for the electric field in the paraxial approximation

$$\begin{aligned}\boldsymbol{E}^{\mathrm{par}}(\mathcal{D}_\varphi\boldsymbol{r},\omega) &= \boldsymbol{E}^{\mathrm{par}}\left[\boldsymbol{E}_0(\mathcal{D}_\varphi\boldsymbol{r},\omega),\, f(\mathcal{D}_\varphi\boldsymbol{r})\right],\\ \boldsymbol{E}^{\mathrm{par}}(\mathcal{M}\boldsymbol{r},\omega) &= \boldsymbol{E}^{\mathrm{par}}\left[\boldsymbol{E}_0(\mathcal{M}\boldsymbol{r},\omega),\, f(\mathcal{M}\boldsymbol{r})\right].\end{aligned}\tag{9}$$

To derive (9), we made the substitutions $\boldsymbol{r}'\rightarrow\mathcal{D}_\varphi\boldsymbol{r}'$ and $\boldsymbol{r}'\rightarrow\mathcal{M}\boldsymbol{r}'$ for the dummy integration variable respectively. For a normally incident plane wave $\boldsymbol{E}_0(\mathcal{D}_\varphi\boldsymbol{r},\omega)=\boldsymbol{E}_0(\mathcal{M}\boldsymbol{r},\omega)=\boldsymbol{E}_0(\boldsymbol{r},\omega)$ is invariant under rotations or the mirror operation, independent of its polarization state. Thus, the scattered electric field within the paraxial approximation reflects all symmetry properties of the PCS, as does the normal component of the Poynting vector since the normal component of the gradient operator is invariant under in-plane rotations or reflections.

Turning next to the symmetry properties of the field including the non-paraxial terms we notice that the non-diagonal elements of the Green tensor couple different polarization components, such that an initially linearly polarized light beam will experience a partial polarization conversion. Thus, an FM obtained in a cross-polarization arrangement shows corrections beyond the paraxial approximation. Applying $\mathcal{D}_\varphi^{-1}$, respectively $\mathcal{M}^{-1}$ to (6) and inserting the transformation properties properties of the full Green tensor

$$\mathcal{D}_\varphi^{-1}\underline{\underline{G}}(\mathcal{D}_\varphi\boldsymbol{r},\omega)\mathcal{D}_\varphi=\underline{\underline{G}}(\boldsymbol{r},\omega)\tag{10}$$

$$\mathcal{M}^{-1}\underline{\underline{G}}(\mathcal{M}\boldsymbol{r},\omega)\mathcal{M}=\underline{\underline{G}}(\boldsymbol{r},\omega)\,,\tag{11}$$

we obtain the transformed functional relations

$$\begin{aligned}\mathcal{D}_\varphi^{-1}\boldsymbol{E}(\mathcal{D}_\varphi\boldsymbol{r},\omega)&=\mathcal{D}_\varphi^{-1}\boldsymbol{E}\left[\mathcal{D}_\varphi^{-1}\boldsymbol{E}_0(\mathcal{D}_\varphi\boldsymbol{r},\omega),\, f(\mathcal{D}_\varphi\boldsymbol{r})\right],\\ \mathcal{M}^{-1}\boldsymbol{E}(\mathcal{M}\boldsymbol{r},\omega)&=\mathcal{M}^{-1}\boldsymbol{E}\left[\mathcal{M}^{-1}\boldsymbol{E}_0(\mathcal{M}\boldsymbol{r},\omega),\, f(\mathcal{M}\boldsymbol{r})\right].\end{aligned}\tag{12}$$

The FM obeys rotational symmetry, if $\boldsymbol{n}\cdot\boldsymbol{S}(\boldsymbol{r},\omega)=\boldsymbol{n}\cdot\boldsymbol{S}(\mathcal{D}_\varphi\boldsymbol{r},\omega)$. If the scattered field gathers components normal to the PCS, the second term on the RHS of (5) also contributes and the flow map displays rotational symmetry only if both $|\boldsymbol{E}(\mathcal{D}_\varphi\boldsymbol{r})|^2=|\boldsymbol{E}(\boldsymbol{r})|^2$ and $\boldsymbol{n}\cdot\left[\boldsymbol{E}^*(\mathcal{D}_\varphi\boldsymbol{r})\cdot(\mathcal{D}_\varphi^{-1}\nabla)\right]\boldsymbol{E}(\mathcal{D}_\varphi\boldsymbol{r})=\boldsymbol{n}\cdot(\boldsymbol{E}^*(\boldsymbol{r})\cdot\nabla)\boldsymbol{E}(\boldsymbol{r})$. These conditions can only be fulfilled if the electric field is an eigenstate of the rotation operator to a complex eigenvalue on the unit circle, i.e., $\mathcal{D}_\varphi^{-1}\boldsymbol{E}(\mathcal{D}_\varphi\boldsymbol{r})=\lambda\boldsymbol{E}(\boldsymbol{r})$. From (6), it can be seen that $\lambda\boldsymbol{E}(\boldsymbol{r})=\boldsymbol{E}\left[\lambda\boldsymbol{E}_0(\boldsymbol{r}),\, f(\boldsymbol{r})\right]$. Obviously, the total electric field displays arbitrary (discrete) rotational symmetries of the PCS if and only if the initial state is also an eigenstate of the rotation operator $\mathcal{D}_\varphi^{-1}\boldsymbol{E}_0(\mathcal{D}_\varphi\boldsymbol{r})=\lambda\boldsymbol{E}_0(\boldsymbol{r})$ to the same eigenvalue. These initial states are the right- and left-handed circularly polarized states with eigenvalues $\lambda_\pm=\exp(\mp\mathrm{i}\varphi)$. Only if the angle of rotation is an integer multiple of π, the eigenvalues are degenerate and arbitrary linear superpositions of left and right-handed circularly polarized states are eigenstates of the corresponding rotation operator. Thus, for an arbitrarily polarized state, the FM exhibits only a twofold rotational symmetry, provided the underlying structure exhibits a $2n$-fold rotational symmetry. These results are in perfect agreement with our numerical findings.

Similarly, enantiomeric symmetry of the FM requires $\mathcal{M}^{-1}\boldsymbol{E}(\mathcal{M}\boldsymbol{r})=\lambda\boldsymbol{E}_{\mathcal{R}}(\boldsymbol{r})$, where $\boldsymbol{E}_{\mathcal{R}}\equiv\boldsymbol{E}\left[\boldsymbol{E}_0,\, f(\mathcal{M}\boldsymbol{r})\right]$ is the field obtained if the enantiomer is excited with the same initial polarization. This condition is fulfilled if and only if the initial state is an eigenstate of the mirror operator that connects the two enantiomeric structures. These are the states polarized parallel or perpendicular to the line of reflection with the eigenvalues $\lambda=\pm1$, respectively. For an arbitrarily polarized state, the enantiomeric symmetry is broken. In particular, for a circularly polarized state, $\mathcal{M}^{-1}\boldsymbol{E}_0^{\pm}\propto\boldsymbol{E}_0^{\mp}$, we have $\boldsymbol{E}^{\pm}(\mathcal{M}\boldsymbol{r})=\boldsymbol{E}\left[\boldsymbol{E}_0^{\mp},\, f(\mathcal{M}\boldsymbol{r})\right]\neq\boldsymbol{E}_{\mathcal{R}}^{\pm}(\boldsymbol{r})$. Instead, the enantiomeric symmetry is recovered if the handedness of the chiral structure and the exciting light field are reversed simultaneously.

Altogether, the analytical considerations presented here are in full agreement with our performed numerical simulations for all kinds of polarization states of the exciting light field. However, it should be noted that the lack of mirror symmetry for linearly polarized light which has been observed in the experiment of [2] cannot be reproduced by our simple model assumptions. By means of a linear isotropic optical response function of the material, enantiomeric symmetry is always conserved if the sample is excited with incident light polarized parallel or perpendicular to the symmetry axis connecting the enantiomers. This symmetry property is also conserved if we insert a truly two-dimensional anisotropic susceptibility where the anisotropy results from the patterning of the structure itself. In this case, the susceptibility of the enantiomer is obtained as $\underline{\underline{\chi}}_{\mathcal{R}}(\boldsymbol{r})=\mathcal{M}^{-1}\underline{\underline{\chi}}(\mathcal{M}\boldsymbol{r})\mathcal{M}$ and transforms in the same manner as the full Green tensor.

4 Polarization coupling

The analytic considerations of the last section showed explicitly that polarization coupling due to the non-paraxial terms is a key ingredient underpinning the broken enantiomeric symmetry observed for circularly polarized fields. However, the model employed here of a locally isotropic and non-magnetic medium would seem to disallow polarization coupling since the induced polarization and electric field are by necessity in the same direction. In this section we discuss how polarization coupling can arise within our model, and this will also give an alternative view of the non-paraxial contributions and the polarization coupling that results from use of the tensorial Greens function.

We start from (3) written in the form

$$\nabla^2\boldsymbol{E}-\nabla(\nabla\cdot\boldsymbol{E})+\frac{\omega^2}{c^2}\boldsymbol{E}=-\mu_0\omega^2\boldsymbol{P}(\boldsymbol{r},\omega)\,,\tag{13}$$

where the polarization is given by $\boldsymbol{P}(\boldsymbol{r},\omega)=\varepsilon_0 f(\boldsymbol{r})\chi(\omega)\cdot\boldsymbol{E}(\boldsymbol{r},\omega)$. According to Helmholtz theorem, the electric field can generally be decomposed into transverse ($\perp$) and longitudinal ($||$) components $\boldsymbol{E}=\boldsymbol{E}_\perp+\boldsymbol{E}_{||}$, with $\nabla\cdot\boldsymbol{E}_\perp=0$ and $\nabla\times\boldsymbol{E}_{||}=0$. Furthermore, in the regions of vacuum outside the PCS where the fields are measured experimentally the

field is strictly transverse. For this reason we seek the wave equation for the transverse part of the field alone. This may be accomplished using the transverse delta-function $\delta_{ij}^{\perp}(\boldsymbol{s})$ to project out the transverse part of a field $\boldsymbol{V}$, in terms of which the transverse part of the vector field can be calculated from the total field as

$$V_{\perp,i}(\boldsymbol{r},t) = \sum_j \int \mathrm{d}^3\boldsymbol{r}' \delta_{ij}^{\perp}(\boldsymbol{s}) V_j(\boldsymbol{r}',t)\,, \tag{14}$$

with $i, j = x, y, z$ and $\boldsymbol{s} = \boldsymbol{r} - \boldsymbol{r}'$. The transverse delta-function has the explicit form [9]

$$\delta_{ij}^{\perp}(\boldsymbol{s}) = \delta_{ij}\delta(\boldsymbol{s}) + \frac{1}{4\pi s}\frac{\partial^2}{\partial s_i \partial s_j}\,, \tag{15}$$

and for a purely transverse field we have the relation

$$0 = \sum_j \int \mathrm{d}^3\boldsymbol{r}' \frac{1}{4\pi s}\frac{\partial^2}{\partial s_i \partial s_j} V_{\perp,j}(\boldsymbol{r}',t)\,. \tag{16}$$

We note that projecting out the transverse part of a field is a non-local operation involving a space integration, and also causes coupling of the vector components since the transverse delta-function is not diagonal in Cartesian indices.

By taking the transverse field projection of (13) we obtain

$$\left[\nabla^2 + \frac{\omega^2}{c^2}\right] E_{\perp,i} = -\mu_0\omega^2 P_{\perp,i}(\boldsymbol{r},\omega)\,, \tag{17}$$

where

$$P_{\perp,i}(\boldsymbol{r},\omega) = \sum_j \int \mathrm{d}^3\boldsymbol{r}' \delta_{ij}^{\perp}(\boldsymbol{s})\varepsilon_0 f(\boldsymbol{r}')\chi(\omega) \times [\boldsymbol{E}_{\perp,j}(\boldsymbol{r}',\omega) + \boldsymbol{E}_{||,j}(\boldsymbol{r}',\omega)]\,. \tag{18}$$

Using the explicit form for the transverse delta-function in (15), one may write the polarization as the sum of local and non-local contributions

$$P_{\perp,i}(\boldsymbol{r},\omega) = \varepsilon_0 f(\boldsymbol{r})\chi(\omega)[\boldsymbol{E}_{\perp,i}(\boldsymbol{r},\omega) + \boldsymbol{E}_{||,i}(\boldsymbol{r},\omega)] - \sum_j \int \mathrm{d}^3\boldsymbol{r}' \frac{\varepsilon_0}{4\pi s}\frac{\partial^2}{\partial s_i \partial s_j}\boldsymbol{E}_{||,j}(\boldsymbol{r}',\omega)\,, \tag{19}$$

where in the last line use was made of (16) and the fact that the electric displacement $\boldsymbol{D} = \varepsilon_0\boldsymbol{E} + \boldsymbol{P}$ is purely transverse.

In (19) that describes the experimentally significant transverse component of the optical response the first term stands for a local response with no polarization conversion. The second, non-local term engages only the longitudinal component of the field and polarization coupling takes place only because of this term. This contribution has a form reminiscent of that describing second order non-locality in crystal optics [10]. We note that in absence of any patterning ($f(\boldsymbol{r}) = \text{const.}$) the longitudinal component vanishes and, hence, the nonlocal term. Therefore, polarization coupling and non-locality have common origin and result from the wavelength scale patterning of the PCS. Thus, if the longitudinal fields are neglected, as in the paraxial approximation of Sect. 3, polarization coupling is absent.

5 Conclusions

In conclusion, we have demonstrated both analytically and numerically that light interaction with planar chiral structures depends on the polarization state of the exciting light field. We have shown that for circularly polarized light the enantiomeric symmetry is broken if the PCS is exchanged with its mirror structure while the handedness of the exciting light is kept. For linearly polarized light, images of fourfold chiral structures exhibit only twofold rotational symmetry. The observed sensitivity on the polarization state is only present beyond the paraxial approximation. The effects rely on the inhomogeneous patterning of the structure and the appearance of longitudinal fields within the PCS.

ACKNOWLEDGEMENTS The authors acknowledge the support of the Science and Engineering Research Council (UK), the German National Academic Foundation, Deutsche Forschungsgemeinschaft, and the NSF International US-Germany Cooperative Grant INT 0 128 975. JVM acknowledges support by the Alexander von Humboldt Foundation.

REFERENCES

1 A. Papakostas, A. Potts, D.M. Bagnall, S.L. Prosvirnin, H.J. Coles, N.I. Zheludev, Phys. Rev. Lett. **90**, 107 404 (2003)
2 A.S. Schwanecke, A. Krasavin, D.M. Bagnall, A. Potts, A.V. Zayats, N.I. Zheludev, Phys. Rev. Lett. **91**, 247 404 (2003)
3 T. Vallius, K. Jefimovs, J. Turunen, P. Vahimaa, Y. Svirko, Appl. Phys. Lett. **83**, 234 (2003)
4 D. Bedeaux, M.A. Osipov, J. Vlieger, J. Opt. Soc. Am. A **20**, 2431 (2004)
5 S.L. Prosvirnin, N.I. Zheludev, Phys. Rev. E **71**, 037 603 (2005)
6 A. Taflove, S.C. Hagness, *Computational Electrodynamics: The Finite-Difference Time-Domain Method* (Artech House, Norwood, 1995)
7 V. Dmitriev, Prog. Electromagn. Res. **48**, 145 (2004)
8 M. Lax, W.H. Louisell, W.B. McKnight, Phys. Rev. A **11**, 1365 (1975)
9 C. Cohen-Tannoudji, J. Dupont-Roc, G. Grynberg. *Photons and Atoms* (John Wiley and Sons, New York, 1989) pp. 14–15, 36–42
10 V.M. Agranovitch, V.L. Ginzburg, *Spatial Dispersion in Crystal Optics and the Theory of Excitons* (John Wiley & Sons, London, 1966) Sect. 1.1